Simulation studies for upgrading a high-intensity surface muon beamline at Paul Scherrer Institute

Lu-Ping Zhou[1,2,3,4,*] Xiao-Jie Ni,[4] Zaher Salman,[4] Andreas Suter,[4] Jing-Yu Tang,[1,2,3]
Vjeran Vrankovic,[5] and Thomas Prokscha[4,†]

[1]*Institute of High Energy Physics, CAS, Beijing 100049, China*
[2]*University of Chinese Academy of Sciences, CAS, Beijing 100049, China*
[3]*Spallation Neutron Source Science Center, Dongguan 523803, China*
[4]*Paul Scherrer Institute, Laboratory for Muon Spin Spectroscopy, CH-5232 Villigen PSI, Switzerland*
[5]*Paul Scherrer Institute, Large Research Facilities Division, CH-5232 Villigen PSI, Switzerland*

The μE4-LEM beamline at Paul Scherrer Institute (PSI, Switzerland) is a special muon beamline combining the hybrid-type surface muon beamline μE4 with the low-energy muon (LEM) facility and delivers μ^+ with tunable energy up to 30 keV for low-energy muon spin rotation (LE-μSR) experiments. We investigate a possible upgrade scenario for the surface muon beamline μE4 by replacing the last set of quadrupole triplets with a special solenoid to obtain 1.4 times the original beam intensity on the LEM muon moderator target. In order to avoid the muon beam intensity loss at the LEM spectrometer due to the stray magnetic field of the solenoid, three kinds of solenoid models have been explored and the stray field of the solenoid at the LEM facility is finally reduced to the magnitude of the geomagnetic field. A more radical design, "Super-μE4," has also been investigated for further increasing the brightness of the low-energy muon beam, where we make use of the current μE4 channel and all sets of quadrupole triplets are replaced by large aperture solenoids. Together with the new slanted muon target E, at least 2.9 times the original muon beam intensity can be expected in the Super-μE4 beamline. Our work demonstrates the feasibility of upgrading surface muon beamlines by replacing quadrupole magnets with normal-conducting solenoids, resulting in higher muon rates and smaller beam spot sizes.

DOI: 10.1103/PhysRevAccelBeams.25.051601

I. INTRODUCTION

The hybrid-type surface muon beamline μE4 at Paul Scherrer Institute (PSI, Switzerland) has already been in operation for more than a decade. The μE4 beamline was first built in the 1970s as a decay muon channel, then rebuilt in 2003 and 2004 as a high-intensity surface muon beamline together with the low-energy muon (LEM) facility [1–7]. Figure 1 shows the layout of the μE4 beamline. Although originally designed to have the ability of transmitting both surface and decay muon beams, the new μE4 beamline has been operating in the surface muon mode and the structure remained unchanged since then. Two normal-conducting solenoids WSX61 and WSX62 close to the muon production target E serve to increase the acceptance, and the following large-aperture magnetic quadrupoles and

dipoles transport the surface muon beam to the LEM moderator. The overall acceptance is limited to around 135 msr due to the employment of quadrupoles and dipoles. The beam momentum is selected by dipoles and the contamination of cloud muons is 5%–10% [3], causing a reduction of beam polarization to about 95%. The Wien filter SEP61 rotates the muon spin by about 10° before being focused onto the muon moderator target in the LEM apparatus. The muon beam is moderated subsequently to a mean energy of about 15 eV in a cryogenic moderator layer of solid argon (or solid neon), deposited on a 125-μm thick Ag foil [8], with an efficiency of $\sim 6 \times 10^{-5}$ ($\sim 1 \times 10^{-4}$ for solid neon). The produced low-energy muons are reaccelerated up to 20 keV and then transported and focused by three electrostatic Einzel lenses and a conical lens [9] to the final sample position, where the beam energy can be tuned in the range from 1 to 30 keV by applying an electrostatic bias to the sample to conduct low-energy μSR (LE-μSR) experiments. Figure 2 shows the layout of the LEM facility [10]. During the beam transport, a spin rotator (Wien filter) is used to rotate the muon spin and to separate protons from the muon beam. These protons originate from the muon moderator by impact ionization of water or hydrogen molecules sticking at the moderator surface.
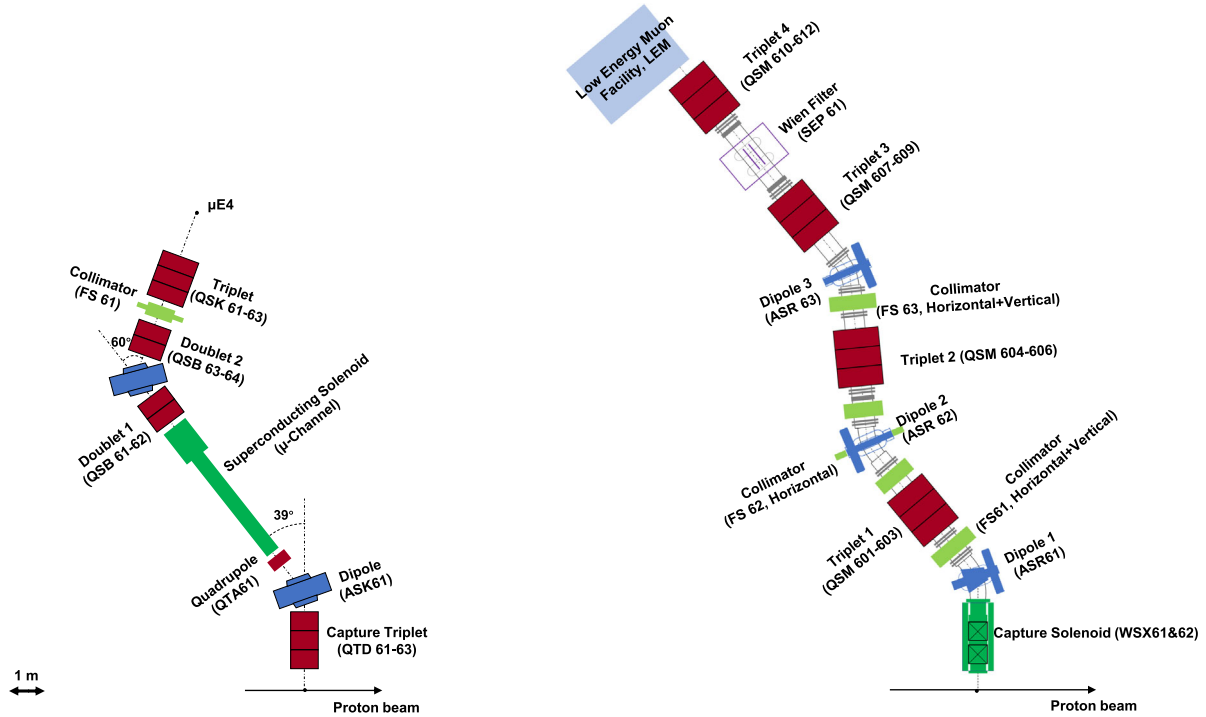
FIG. 1.   Left: the old μE4 decay channel; Right: the hybrid-type μE4 beamline rebuilt in 2003 and 2004 as a surface muon injector for the LEM facility.

In recent years, most of muon beamlines around the world have been further upgraded to obtain better performances. In the United Kingdom, the ISIS Neutron and Muon Source (ISIS) has developed its muon beamline at the EC muon facility by replacing doublets with

FIG. 2.   The layout of LEM facility.

large-aperture triplets and got about a factor of 2 increase in muon rate and a beam spot with 0.6 cm rms radius in the simulation [11,12]. In Japan, the RCNP of Osaka University has built the MuSIC muon beamline for the verification of a beamline fully based on the solenoid capture and transport for muon physics experiments such as Coherent Muon to Electron Transition (COMET) at Japan Proton Accelerator Research Complex (J-PARC) [13], and later transformed for μSR applications [14,15]. Newly designed surface muon beamlines are more likely to use large aperture solenoids to increase the beam intensity on the sample. For instance, J-PARC in Japan has succeeded to build the second slow muon beamline in the world, the Ultra Slow muon beamline (USM). It uses the so-called Super Omega beamline, which is mainly composed of solenoids [16–19], to supply a high-intensity surface muon beam for USM generation. On the opposite side of the muon target station, J-PARC prepares to use large aperture capture solenoids to increase the acceptance of its H-line and then transport the high-intensity muon beam by using a pair of two solenoids that have reverse currents [20,21]. In Switzerland, PSI is investigating new high-intensity muon beams (HIMBs) with a surface muon rate up to 10^{10}/s based on its new target M (so-called target H) [22–24]. In China, the first muon source experimental muon source (EMuS) is going to is going to use solenoids to transport high-intensity surface muon and pion beams in the baseline scenario [25].

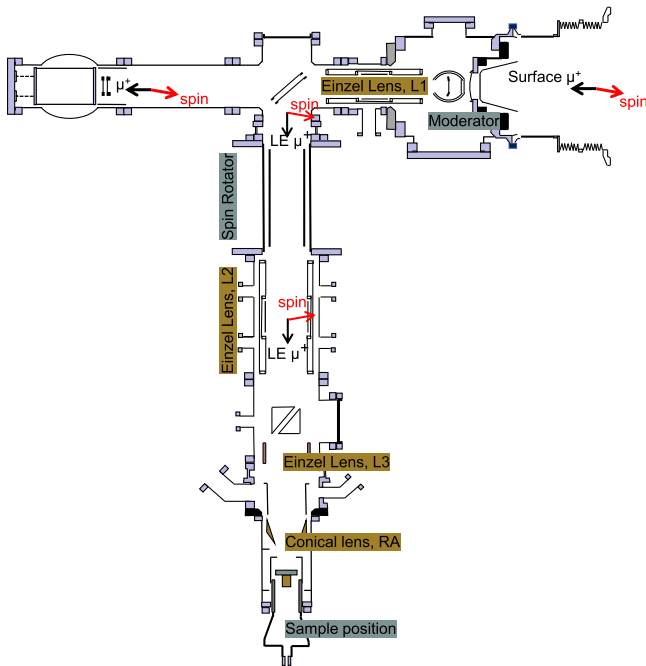At PSI, the existing μE4 beamline, using large aperture quadrupole triplets for beam transport, can deliver about

40% of the surface muon beam onto the rectangular moderator target with a size of 30×30 mm^2. The causes for low transmission efficiency are (i) the large transverse emittances of $\varepsilon_x = 550\,\pi$ cm mrad and $\varepsilon_y = 1000\,\pi$ cm mrad, and (ii) the asymmetric focusing in x and y directions of the last quadrupole triplet, causing an asymmetric beam spot on the moderator with respective x- and y-rms values of $\sigma_x = 2.9$ cm and $\sigma_y = 1.4$ cm [3]. These two beam characteristics limit the rate of moderated muons to 1.2×10^4/s (solid argon) and 2.0×10^4/s (solid neon) at a proton beam current of 2 mA. An increase in these rates will have a large positive impact on the entire user program at the LEM facility. We therefore started a study to increase the muon beam intensity and to reduce the beam spot size due to the large transverse emittances and asymmetric focusing. As a first step, replacing the last quadrupole by a solenoid can already significantly improve the beam spot on the moderator. However, a solenoid generates extended stray magnetic fields, which will seriously deteriorate the transport of the low-energy muon beam after moderation. Thus, the solenoid has to be designed with a sufficiently small residual stray field at the LEM facility to avoid significantly distorting the transmission of the low-energy muon beam to the LE-μSR spectrometer, while keeping the ability of focusing the muon beam on the moderator. In a second step, the replacement of all quadrupole triplets by solenoids is investigated (Super-μE4), which gives the largest possible improvement of the beam transport of μE4.

This paper is organized as follows: Sec. II introduces the μE4 beam simulations and the comparison between utilizing a solenoid or a quadrupole triplet for the final focusing, followed by Sec. III, where we introduce the exploration of the possible solenoid models with low stray field and their impact on the muon beam transport to the LE-μSR spectrometer. In Sec. IV, we introduce the high-intensity muon beamline Super-μE4 study based on large aperture normal-conducting solenoids.

II. SIMULATIONS FOR DIFFERENT DESIGNS OF THE MUON TARGETS AND BEAMLINES

The two pion and muon production targets "M" and "E" of the PSI High Intensity Proton Accelerator (HIPA) facility are slowly rotating graphite wheels, with a straight pion and muon production volume in the proton beam direction and lengths of 5 and 40 mm, respectively [26]. Recent studies of the muon production target E at PSI have revealed that a slanted target E, with the same effective length for the proton beam as the original straight target, can yield a 30%–40% increase of surface muon beam rate by sideway collection depending on different target rotation angles [23,26]. This increase is mainly caused by the effectively larger surface and production volume of this target geometry. In the studies of μE4, G4beamline [27] is

used to simulate both the production of pions and muons in target E and the transport of the surface muons through the beamline. G4beamline uses Geant4 cross section models for pion production, yielding relatively larger or smaller rates of surface muons depending on different physics models (Ref. [26] offers the corrected cross section). The detailed simulation of pion and muon production in the target, however, exceeds the scope of this paper since we are mainly interested in studying the relative increase of surface muon beam rate with a simplified generation of the source particles for the beamline simulation. The parameters of the target and proton beam are taken from Ref. [26]. The rms values of the incident proton beam at the target are $\sigma_x = 0.75$ mm and $\sigma_y = 1.25$ mm, and Fig. 3 shows the two target geometries used in the simulation. The original, 40-mm long straight target E (OTE) is simulated as a rectangular graphite box of 40 mm length, 6 mm width, and 100 mm height. The parameters of the new slanted target E (NTE) are simulated as a rectangular graphite box of 83.5 mm length, 5.56 mm width, and 100 mm height, with an 8-degree rotation around the vertical axis y. Only muons originating in the region -20 mm $< y < 20$ mm are taken into consideration for both targets because of their wheel-like shape [26]. The initial phase spaces of the muon beam produced by the two targets are shown in Fig. 4. Using in G4beamline the model QGSP_BIC for pion production in target E, the experimentally observed muon rates at the end of the μE4 beamline are fairly well reproduced, see the Appendix.
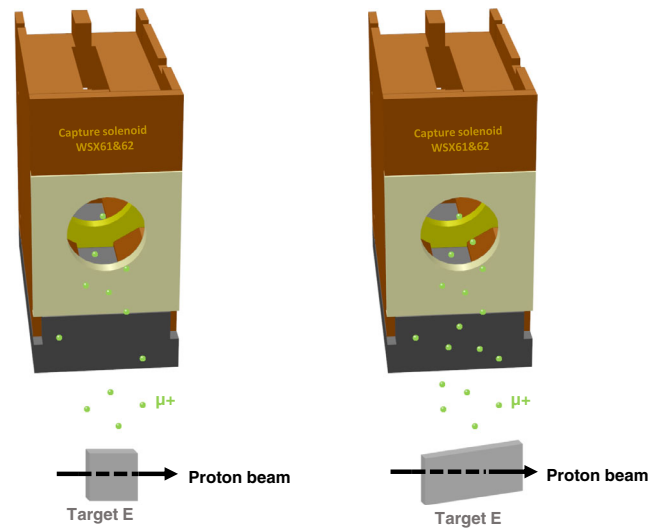

FIG. 3. The OTE, as shown on the left side, has been replaced by the NTE in November 2019, shown in the right figure. The two targets are designed to have the same effective length for the proton beam to ensure that energy loss, scattering, and the deposited power of the beam in the target remain unchanged while the new target has a larger surface producing more surface muons. In order to see the difference more clearly, both targets have been magnified proportionally.
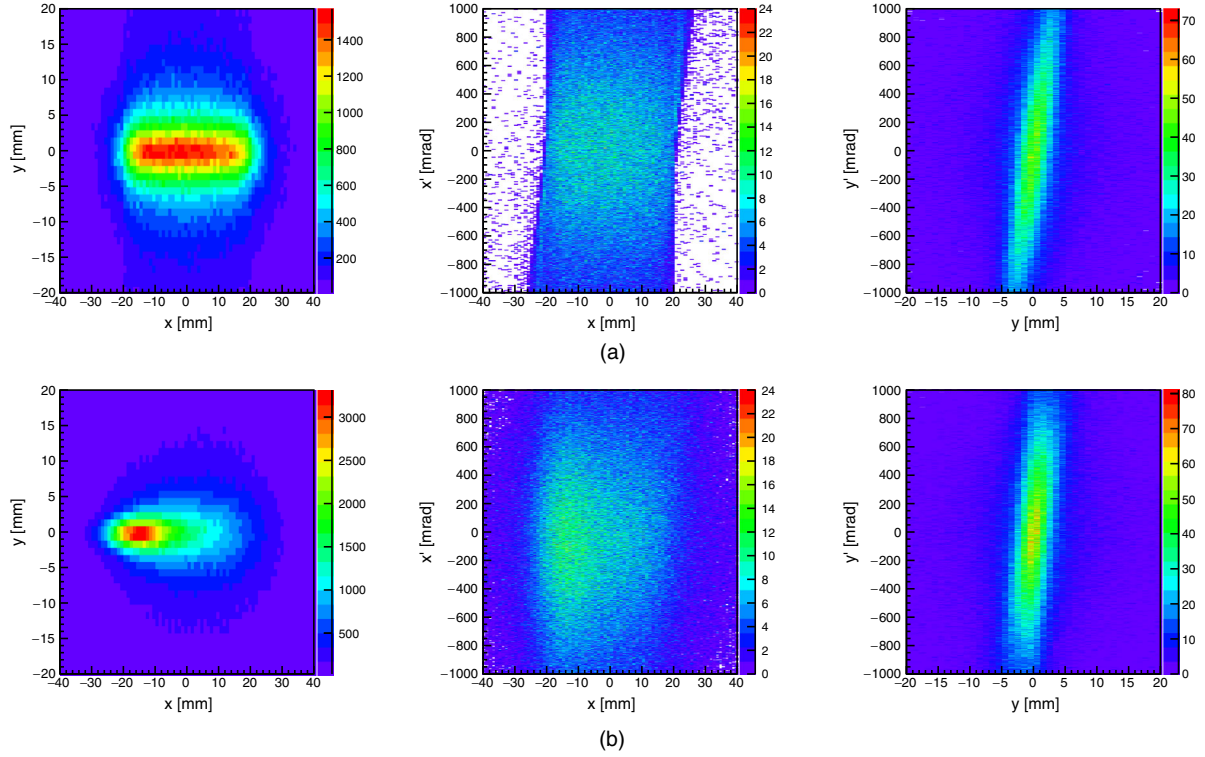
FIG. 4.   (a) Real space (x-y) distribution and phase spaces (x-x' and y-y') of the OTE. (b) Corresponding distributions of the NTE. Virtual detectors are attached to the surface of the target to record surface muons in the simulation. 10^{11} protons are simulated for each target and we use "QGSP_BIC" as the physical model for the interaction of the proton beam for both target simulations in G4beamline.

Due to the higher order effects, both focusing by the large aperture quadrupole triplets and the solenoid will introduce a distortion of transverse phase spaces for the beam with both transverse emittances being of the order of 100 π cm mrad. When using the solenoid for transporting and focusing of the large emittance beam with a wide momentum spread of a few percent, the higher order effects of the solenoid and the coupling of different planes will probably increase the 4D rms emittance [28]. However, the beam transport benefits from the more symmetric focusing in the two transverse directions, resulting in a smaller beam spot size.

Figure 5 shows the μE4 beam envelope optical calculations using the program TRANSPORT [29], which is based on the calculation of beam transfer matrices. In contrast to the existing μE4, the beam waist at the end of the beamline at the moderator position can be made symmetrical in x and y using a solenoid instead of the last quadrupole triplet. This indicates that a higher beam intensity on the moderator area can be achieved by symmetric focusing. In TRANSPORT, the transfer matrix of solenoids is defined for "long" coils, where the length is much larger than the aperture. In the μE4 case with "short" solenoids, the length is about the same as the aperture. Also, the iron housing of the μE4 solenoids affects the fringe fields of the solenoids, which is not taken into account by the standard transfer matrix for a solenoid in

TRANSPORT. Nevertheless, as has been shown in [3], the transfer matrix formalism gives a sufficiently well description of the beam optics with the short solenoids, which is beneficial for efficient beamline optimization and for a quick and instructive evaluation of the main characteristics of the beamline.

The beam optics is only calculated to second order in TRANSPORT. For the transmission studies of the large emittance beams, including a correct transport through the solenoids, a multiparticle Monte Carlo simulation is therefore indispensable. Therefore in a next step, G4beamline is employed for the simulation of beam transport in which the uniform distribution of the initial phase spaces in TRANSPORT is used as the input beam source. In the Monte Carlo simulation, the fractions of muons transported onto the moderator target of the existing μE4 beamline for different momentum bites are compared with those of the upgraded μE4 beamline, where the last quadrupole triplet is replaced by a simple solenoid named "WSY" with an aperture of 0.4 m and a length of 0.5 m. The field of the G4beamline solenoid model, which is shown in Fig. 6, is calculated based on the Biot-Savart law and represents a real solenoid without any iron housing. Figure 7 shows the simulation results by using the G4beamline solenoid WSY. In the simulation, the existing μE4 beamline can focus 38%–44% of the whole beam on the moderator, depending on the momentum bite.
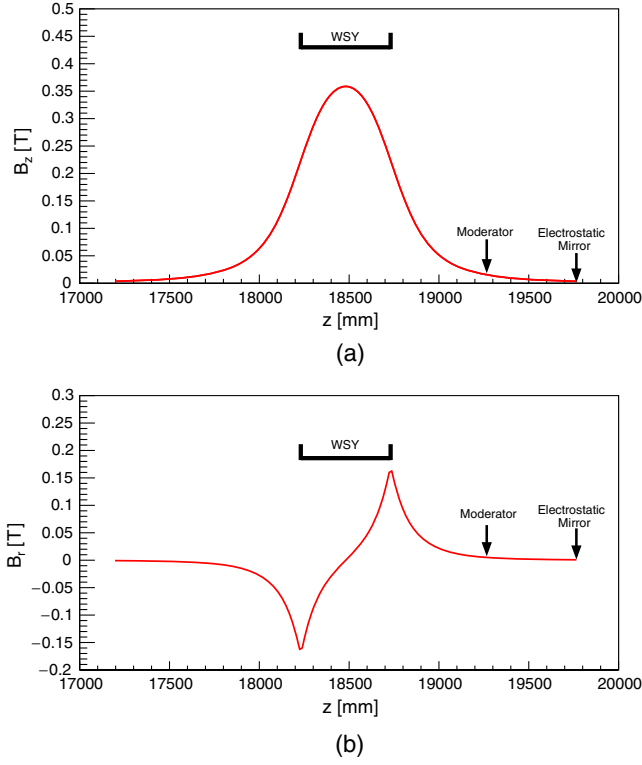
FIG. 5. Beam envelopes calculations of the μE4 beamline using TRANSPORT: (a) Current μE4 beamline; (b) upgraded μE4 beamline with a solenoid replacing the last quadrupole triplet. Initial parameters used in TRANSPORT are (half-width) $x = 20$ mm, $x' = 200$ mrad, $y = 2.5$ mm, $y' = 200$ mrad, $dp/p = 0$ (red lines) and 4.5% (black lines). The red lines indicate the first-order calculations and the black lines are the second-order calculations. The arrows represent the three slit systems with maximum jaw opening.

FIG. 6. The magnetic field of the solenoid used in G4beamline: (a) B_z component along the center line; (b) B_r component at maximum aperture $r = 20$ cm. The field has been tuned to get the maximum intensity on moderator. The horizontal axis shows the position in the beamline. The center of the solenoid WSY is located at $z = 18,481$ mm and moderator is located at $z = 19,266$ mm.

The G4beamline solenoid WSY can focus more muons on the moderator regardless of different momentum bite, where the total transmission efficiency remains almost unchanged since the WSY has the same aperture as the
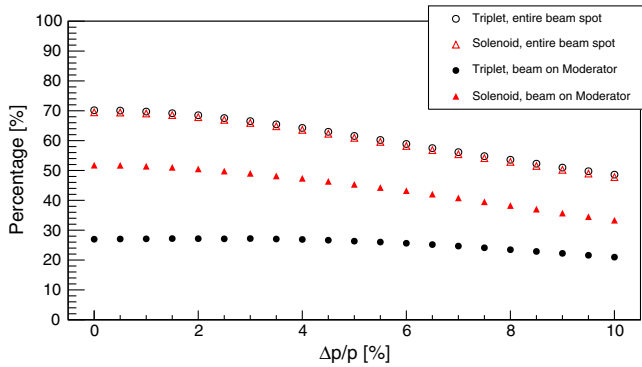
FIG. 7. The fractions of muons with the initial phase spaces used in TRANSPORT that are transported to the position of the moderator in G4beamline for the current μE4 beamline and the upgraded μE4 beamline. 100,000 muons for each momentum bite settings are generated in the simulation at the muon target E. Statistical errors of simulations are less than 1%.

quadrupole magnets. For example, using this simplified initial phase space, $\sim$70% of the beam is focused on the moderator at the full momentum bite of 10% of the μE4 beamline by using WSY.

The simulated beam spots and phase spaces at the moderator position using the initial phase spaces of Fig. 4 for the OTE and the NTE are compared and shown in Fig. 8. To optimize the fraction of muon beam focused on the moderator with a fixed area size (30×30 mm^2), the divergences of the focused beam x' and y' have to be maximized. For obtaining the highest intensity on the moderator, the triplet can generate a beam waist with large divergence in only one direction (y), while the divergence in the other direction (x) is limited to $\sim$100 mrad. In the solenoid case, both divergences x' and y' can reach large values up to 200 mrad (see Fig. 9), and the original rectangle-like shape of the beam spot becomes more like a circle symmetric about x and y, as shown in Fig. 8. The gain in muon rate on the moderator by using the G4beamline solenoid WSY compared with the quadrupole triplet is 52% for the OTE, which is less than the 70% using the simplified initial phase space of the TRANSPORT simulation.

Compared to the OTE, the employment of the NTE in the simulation results in additional increases in muon rate of 33% for the current μE4 beamline by comparing Fig. 8(b) with Fig. 8(a), and 37% for the upgraded μE4 beamline by comparing Fig. 8(d) with Fig. 8(c). The overall increase of muon rate on moderator by using the NTE with larger muon production volume or surface, and by using a solenoid at the end of the beamline amounts to 108% by comparing Fig. 8(d) with Fig. 8(a).

Although the use of the G4beamline solenoid WSY instead of the last quadrupole triplet (QSM610-612) demonstrates a significantly better achievable intensity at the final beam focus, the stray field of this solenoid has a serious influence on any experiment downstream of the beam focus. We will use the LEM facility to study exemplarily the serious influence of these stray fields on a low-energy muon beam. The deflection of the muon in a homogeneous transverse magnetic field can be calculated by the following formula [3]:

$$d(mm) = \int_0^l \varphi_B \, dl = 15 l_B^2 (m) \frac{B(G)}{p(\text{MeV}/c)}, \quad (1)$$

where l_B is the length of the muon trajectory and φ_B is the deflection angle of the muon. The section from the electrostatic mirror to the position of sample (EM-S) of the LEM beamline is 1.678 m, as shown in Fig. 10. The deflection will be $\sim$24 mm for muons with a typical kinetic energy of 15 keV ($p = 1.78$ MeV/c) under 1 G homogeneous field. The overall deflection of the beam spot would be smaller due to the focusing effect of the Einzel lenses and the conical lens. However, the stray
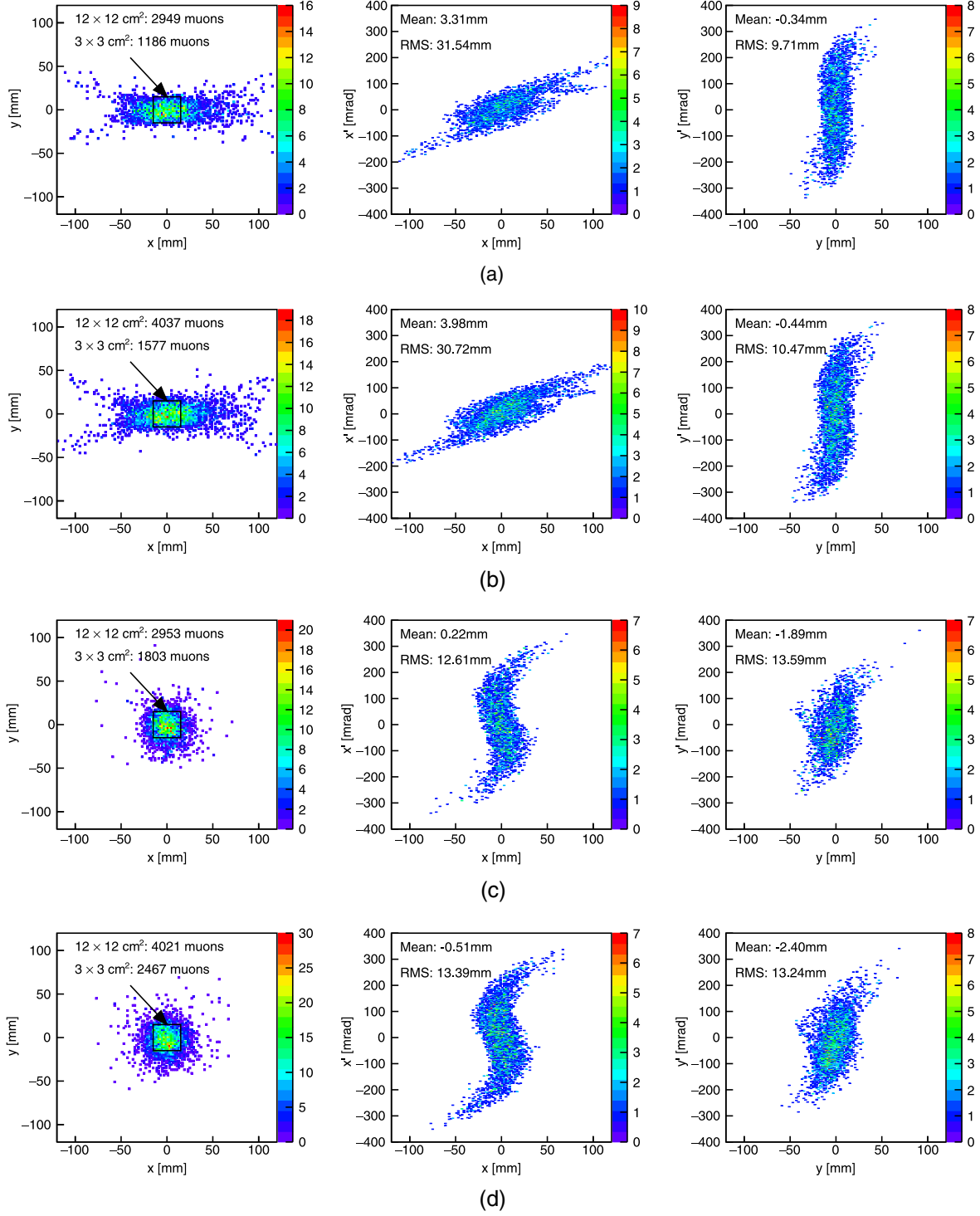
FIG. 8. Simulated beam spots and phase spaces at the LEM moderator position for different muon target E geometries and beamline settings: (a) OTE + quadrupole triplet (i.e., the original setting of the μE4); (b) NTE + quadrupole triplet; (c) OTE + G4beamline solenoid WSY; (d) NTE + G4beamline solenoid WSY. For the NTE simulation, the center of the μE4 beamline is aligned to the center of the muon distribution [$x = -8$ mm in Fig. 4(b)].

field still needs to be shielded below 1 G to keep the muon on the correct trajectory and to minimize rate loss. The stray field component B_z of the G4beamline solenoid WSY without any iron housing along the EM-S beam section is shown in Fig. 11. The maximum value is 35 G when the center field B_0 reaches 3588 G inside the solenoid. From Eq. (1), the low-energy muon beam would be quickly deflected and lost in the EM-S beam
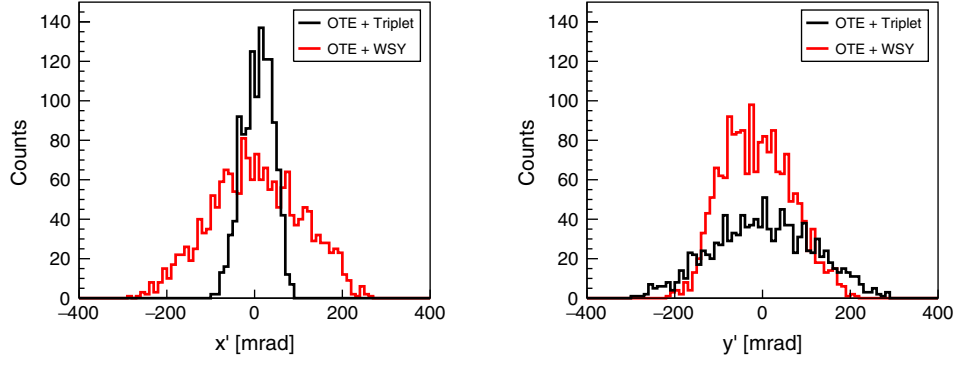
FIG. 9.   Comparisons of the transverse divergences for different beam spots. Left: horizontal direction; right: vertical direction.
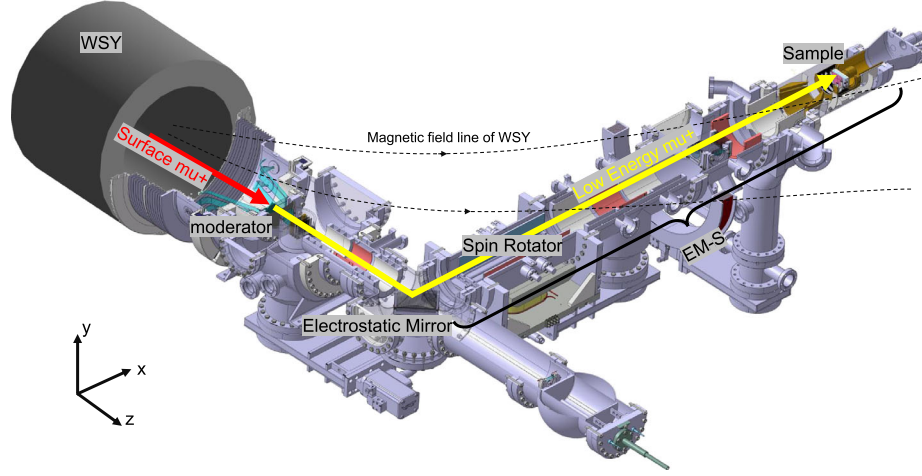

FIG. 10.   Profile of the LEM facility, showing the section EM-S between the electrostatic mirror (EM) and the position of the sample (S), where the LE-μSR experiments are carried out.

section. Therefore, it is necessary to design a special solenoid WSY which does not only satisfy the focusing demands of the μE4 beamline to increase the muon rate on the moderator but also generates sufficiently small stray fields in an acceptable range for the LEM facility, not only on axis but also far off axis.
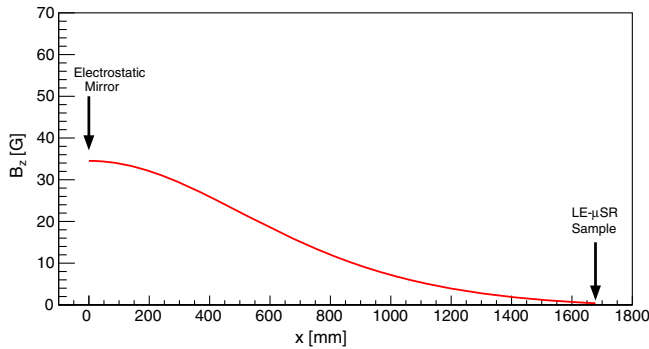
FIG. 11.   Stray field B_z of the G4beamline solenoid WSY along the section EM-S of the LEM facility.

III. INVESTIGATION OF POSSIBLE MODELS FOR THE SOLENOID WSY

Three kinds of models have been investigated in attempting to reduce the stray field in the LEM region. The idea is to either use the iron housing or add compensation coils with reverse current direction on the outside or combine them together. Solenoid models are built and analyzed with the finite element analysis software OPERA [30]. Figure 12 shows the traditional iron housing method that was used in the existing solenoids WSX61/62 of the μE4 beamline. The relatively small moderator area requires accurate focusing of the beam. Any small offset of the solenoid in its position could lead to unacceptable beam losses. The compensation iron inside the solenoid helps ensure the precise installation and enables a more efficient operation. For the strict requirement of the LEM facility, different acceptable sizes of iron housing have been investigated for reducing the stray field component B_z along the EM-S beam section. The analysis results are shown in Fig. 13 and all their focusing powers $\frac{1}{f}$ [31] have been normalized to what is used in the G4beamline
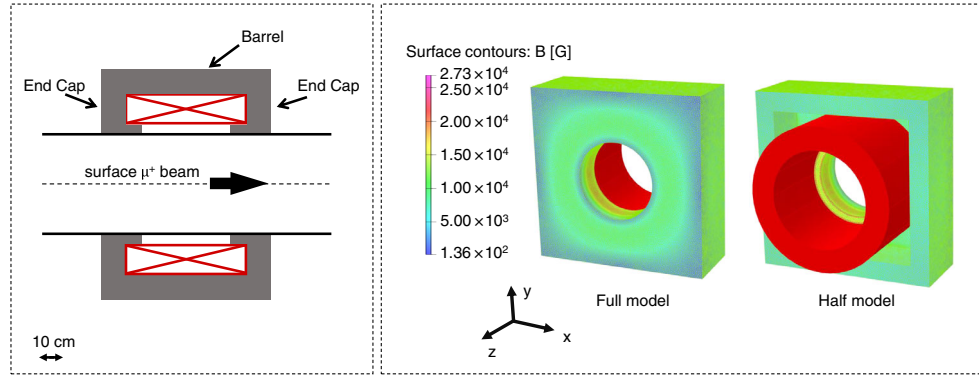
FIG. 12.   Model 1: the typical iron housing solenoid in OPERA.

simulation as mentioned in Fig. 7. The outer iron housing is important to shield the stray field leaking into LEM, as long as it remains unsaturated. In general, the use of the iron housing can reduce the stray field to a few Gauss with acceptable iron thicknesses. Increasing the barrel thickness beyond a certain value does not further reduce the overall stray field at the EM-S beam section. Increasing the

thickness of the end cap is effective for reducing the stray field at the position closer to the end cap, that is, it can reduce the stray field strength at the electrostatic mirror. As the distance from the end cap increases, the shielding ability of the end cap decreases.

The second model investigated is the dual-layer solenoid, which has a main solenoid and an outer solenoid with current in the opposite direction [32,33], see Fig. 14. By varying the ratio of the currents of the two solenoids, the
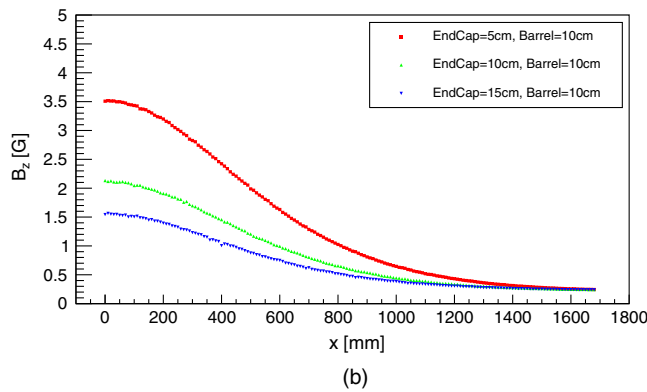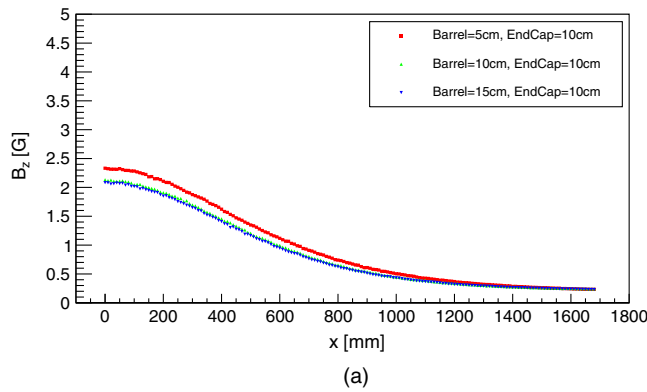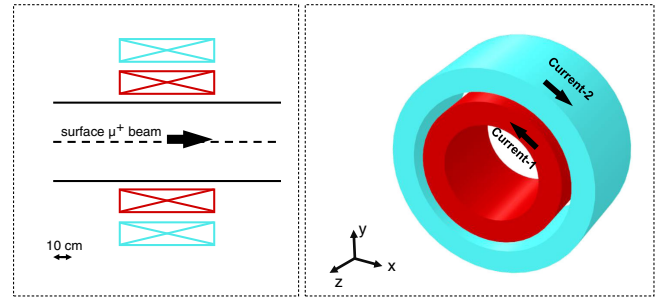

FIG. 14.   Model 2: the dual-layer solenoid. The outer coil has the direction of current opposite to the inner coil (blue: the outside coil, red: the inner coil).
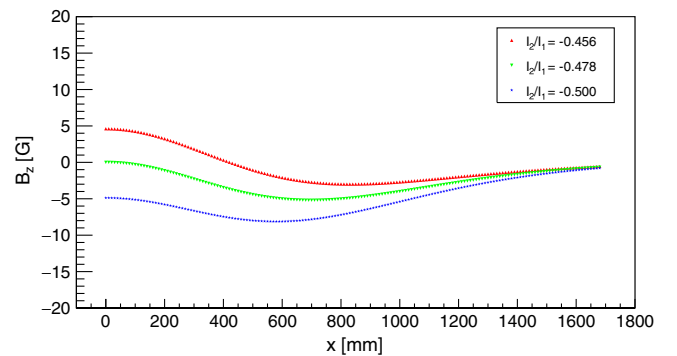

FIG. 13.   Model 1: the stray field component B_z of the solenoid WSY along the EM-S beam section for different thicknesses of the iron housing. (a) WSY with different barrel thicknesses and end cap thicknesses fixed at 10 cm; (b) WSY with different end cap thicknesses and barrel thicknesses fixed at 10 cm.

FIG. 15.   Model 2: stray field B_z along the EM-S beam section for the dual-layer solenoid with different current ratios.
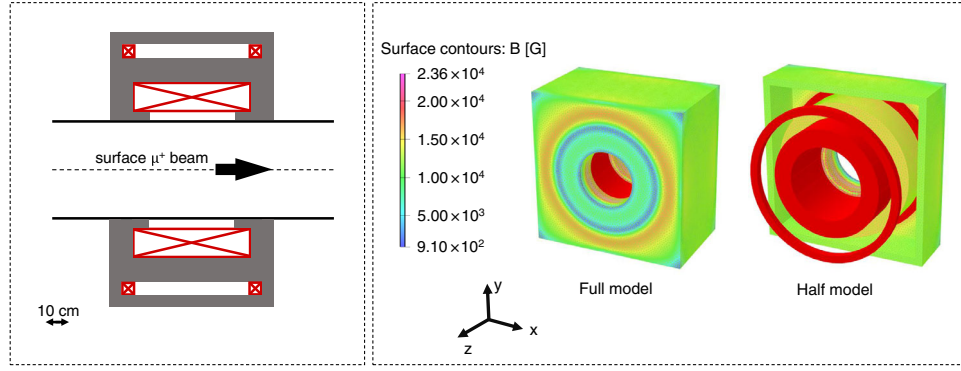
FIG. 16.   Model 3: the iron housing solenoid with compensation coils.

field inside the solenoid and the stray field at the EM-S beam section can be changed. Stray fields with different ratios of currents are shown in Fig. 15. All of their focusing powers have been normalized to what is used in the G4beamline simulation as mentioned in the first model. To achieve optimum focusing on the moderator and minimum stray fields, the inner coil needs to be operated at a high current density exceeding 5 A/mm^2 to compensate the negative effect on the focusing power by the outer coils. This would probably require the use of superconducting technology, since ~5 A/mm^2 is the limit for normal-conducting coils.

At a ratio $I_2/I_1 = -0.478$, the stray field at the position of the electrostatic mirror can be compensated to almost 0. However, the stray field at the middle position of the EM-S beam section still can reach -5 G, and the beam will be lost in the EM-S beam section. Hence, we conclude that the outer coil alone cannot compensate the stray fields to an

acceptable low value along the entire EM-S beam section. Therefore, the third model which combines the first and the second model to further minimize the stray field along the EM-S beam section is investigated, as shown in Fig. 16. This model has been optimized to keep the iron housing unsaturated except the inner iron part located inside the main coil. In order to avoid the superconducting technology
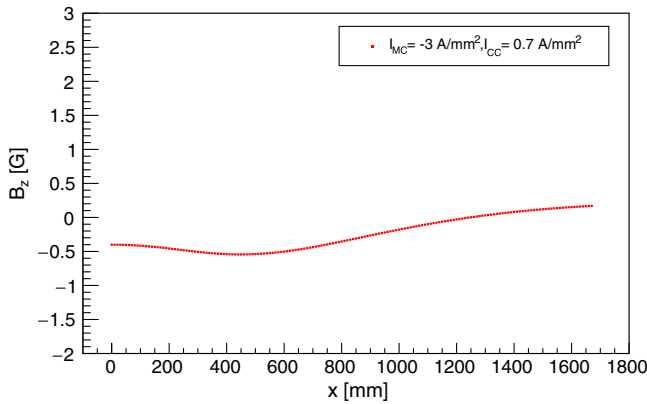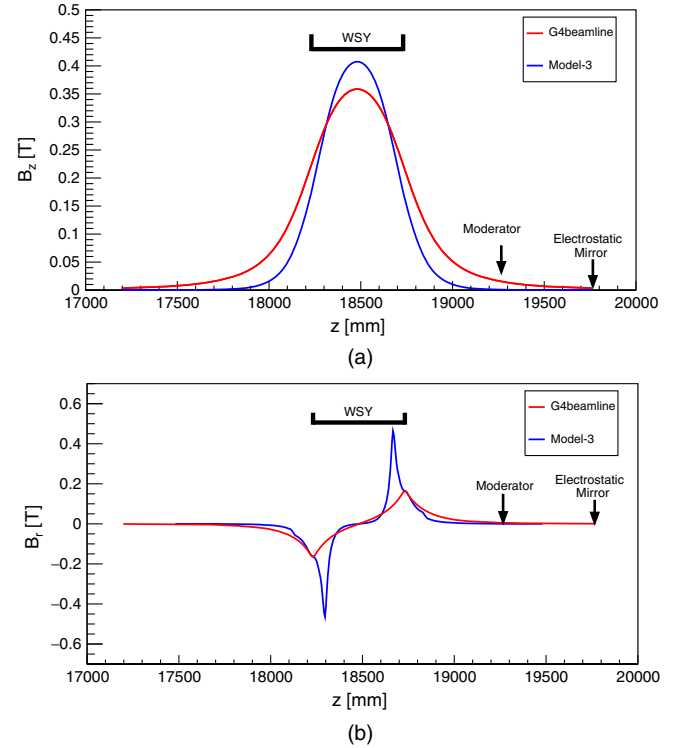

(a)

(b)

FIG. 18.   Comparison of magnetic fields of the G4beamline solenoid and the OPERA model-3: (a) B_z along the solenoid central axis; (b) B_r at the maximum aperture $r = 20$ cm. Both the fields of two solenoids have been normalized to have the same focusing power.

FIG. 17.   Model 3: the stray field B_z along the EM-S beam section. The main coil (MC) works at a current density of 3 A/mm^2 and the compensation coils (CC) work at 0.7 A/mm^2 with opposite current direction.
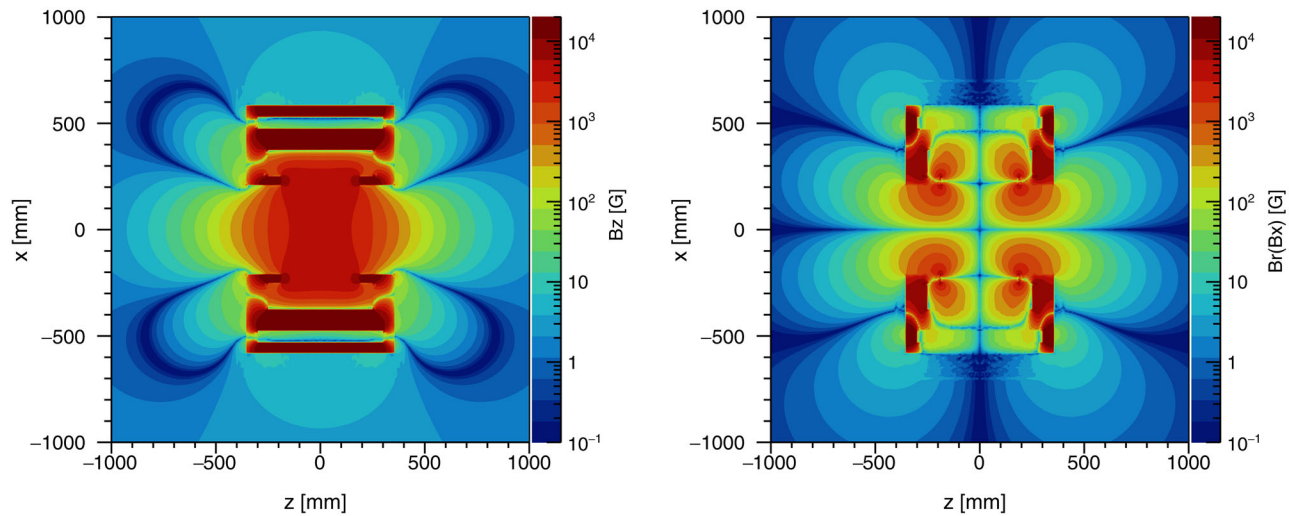
FIG. 19.   Contour map of B_z/B_r on the *XOZ* plane of the model-3 WSY.

and considering the conductor area ratio in the water-cooled wire, all the current densities are kept below 3 A/mm^2. The stray field of this model is shown in Fig. 17 and its focusing power has been normalized as in the previous models. The center field becomes sharper compared to the solenoid center field used in G4beamline, as shown in Fig. 18. The stray field of model-3 along the EM-S beam section reaches the magnitude of the geomagnetic field, which is small enough for a nearly

undisturbed beam transport, as shown below. A contour map of B_z/B_r outside model-3 WSY is shown in Fig. 19.

The model-3 WSY has different performance compared to the G4beamline solenoid due to the shielding of the stray field. Using the OTE in the simulation, the focusing ability
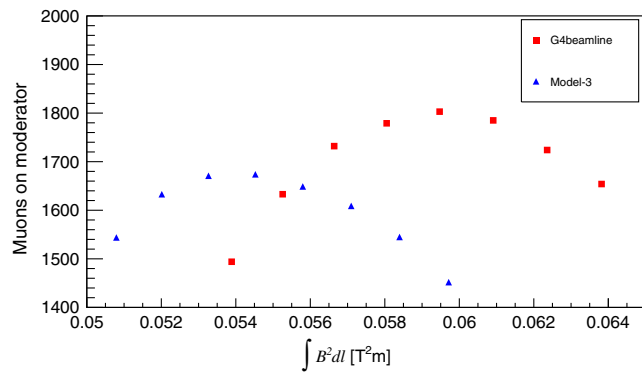

FIG. 20.   Comparison of focusing capabilities of model-3 WSY and G4beamline solenoid by using OTE in the simulation. Red squares show the number of muons on the moderator for the G4beamline solenoid as a function of focusing power (max = 1803 muons). Blue triangles show the result for model-3 WSY (max = 1685 muons).
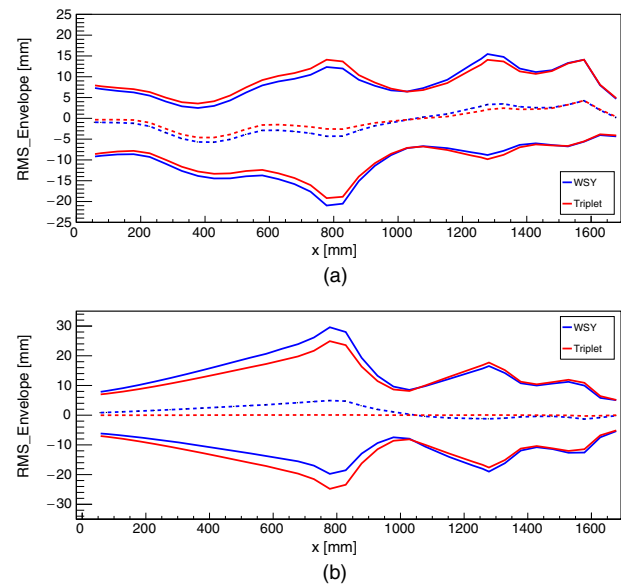
FIG. 21.   Comparisons of (a) horizontal and (b) vertical rms (solid lines) and center (dashed lines) of the beam for the 15-keV muon beam under the influence of different stray fields along the EM-S beam section.
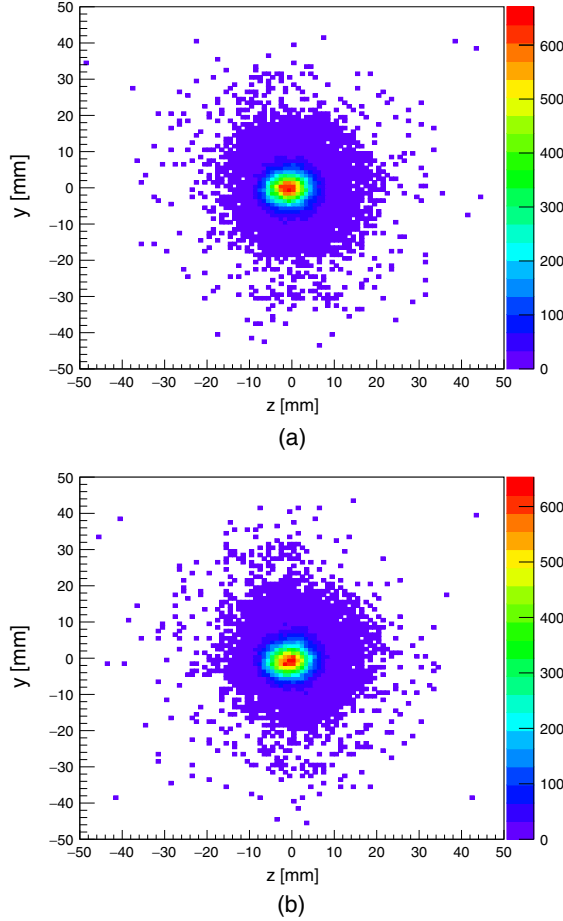
FIG. 22. Comparison of the 15-keV muon beam spots at the sample position under the influence of different stray fields: current μE4 with (a) quadrupole triplet and (b) solenoid WSY, model-3.

of the model-3 solenoid WSY is weaker than that of the G4beamline solenoid by about 7%, as shown in Fig. 20.

For the beam transport of low-energy muons, the influence of the model-3 WSY stray fields along the EM-S beam section is simulated for a typical beam energy of 15 keV using the Geant4-based program MUSRSIM [34]. The rms beam envelopes and beam spots at the sample position of the LE-μSR experiments are shown in Figs. 21 and 22, respectively, calculated for the current LEM beam transport element settings. Table I shows the fraction of the beam in different areas at the sample position for the current μE4 with quadrupole triplet (stray field is zero) and model-3 WSY. Compared with the current beamline, the influence of stray fields of model-3 WSY on the low-energy muon beam can be neglected.

IV. THE HIGH-INTENSITY MUON BEAMLINE SUPER-μE4

As an ultimate—although significantly more expensive—upgrade of the μE4 beamline, the so-called Super-μE4 beamline has been explored, where all quadrupole triplets are replaced by normal-conducting solenoids with an aperture of 500 mm. The optimum beam transport can be achieved with short solenoids, as shown below, and there is no need to use superconductor technology. The Super-μE4 upgrade is an example study of how a beamline with practical constraints due to existing radiation shielding and already specified deflection angles can be further optimized with regard to beam transmission. This beamline is mainly designed for the large surface area of the NTE, therefore the acceptance is designed as 30 mm/200 mrad and 2.5 mm/200 mrad (half widths) for horizontal and vertical directions, respectively. Two options are useful for controlling the beam profile in the solenoid transmission system when considering the first-order beam optics: (i) ensuring the phase space rotation angle by the system is close to $\theta = n\,(\pi/2)$ ($n = 0, 1, 2, \ldots$); (ii) using solenoid pairs instead of a single solenoid, where the first solenoid "couples" transverse phase spaces and the second solenoid "decouples" the phase spaces by employing opposite magnetic fields [3,21]. Figure 23(a) shows the optical calculation for the Super-μE4. The first two solenoids WSX61 and WSX62 rotate the phase space by nearly 90°. Stray fields of the following solenoid pairs S1-1/2 and S2-1/2 as well as the single solenoid M-S are shielded by iron housing as in our WSY model-1 to avoid the superposition of the fields between solenoids and the adjacent dipoles. The M-S solenoid controls the beam envelopes and divergences on entering the $\mathbf{E} \times \mathbf{B}$ separator SEP61 and the focusing solenoid WSY, so that the beam envelopes in WSY are large enough to maximize the divergence of the beam focused on the moderator, thereby maximizing the beam intensity. The uniform initial distribution of the muon beam at target E, as used in TRANSPORT, is used in G4beamline to help tuning and optimizing the fields of the solenoids in the multiparticle simulation. Figure 23(b) shows the rms transverse beam envelopes in G4beamline after tuning the solenoids. The best beam transport has been found for S1-1/S1-2, S2-1/S2-2, and M-S all having same magnetic field direction, opposite to WSX61/62 and WSY.

Simulated beam spots and divergences of the beam focused on the moderator are shown in Figs. 24 and 25, respectively. Table II summarizes the muon intensities on the total beam spot (12×12 cm^2) and the moderator (3×3 cm^2) for different target and beamline settings. While the upgraded μE4 (model-3 WSY) increases the

TABLE I. Comparison of beam spot fractions at the LEM sample position for different stray fields using 10 000 simulated muons starting at the moderator.

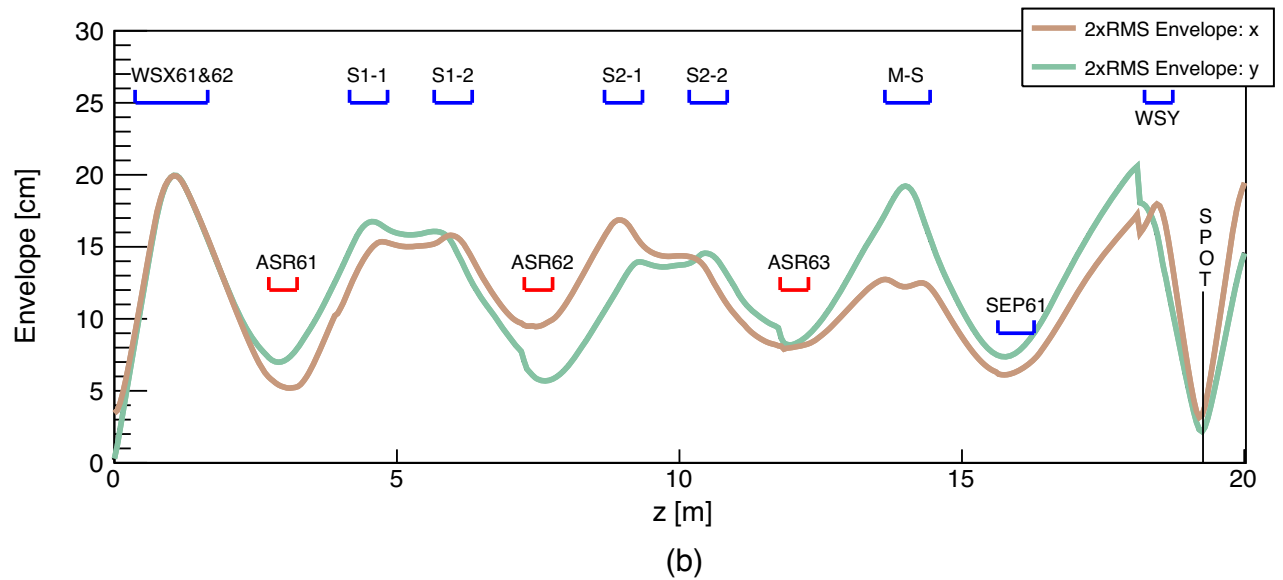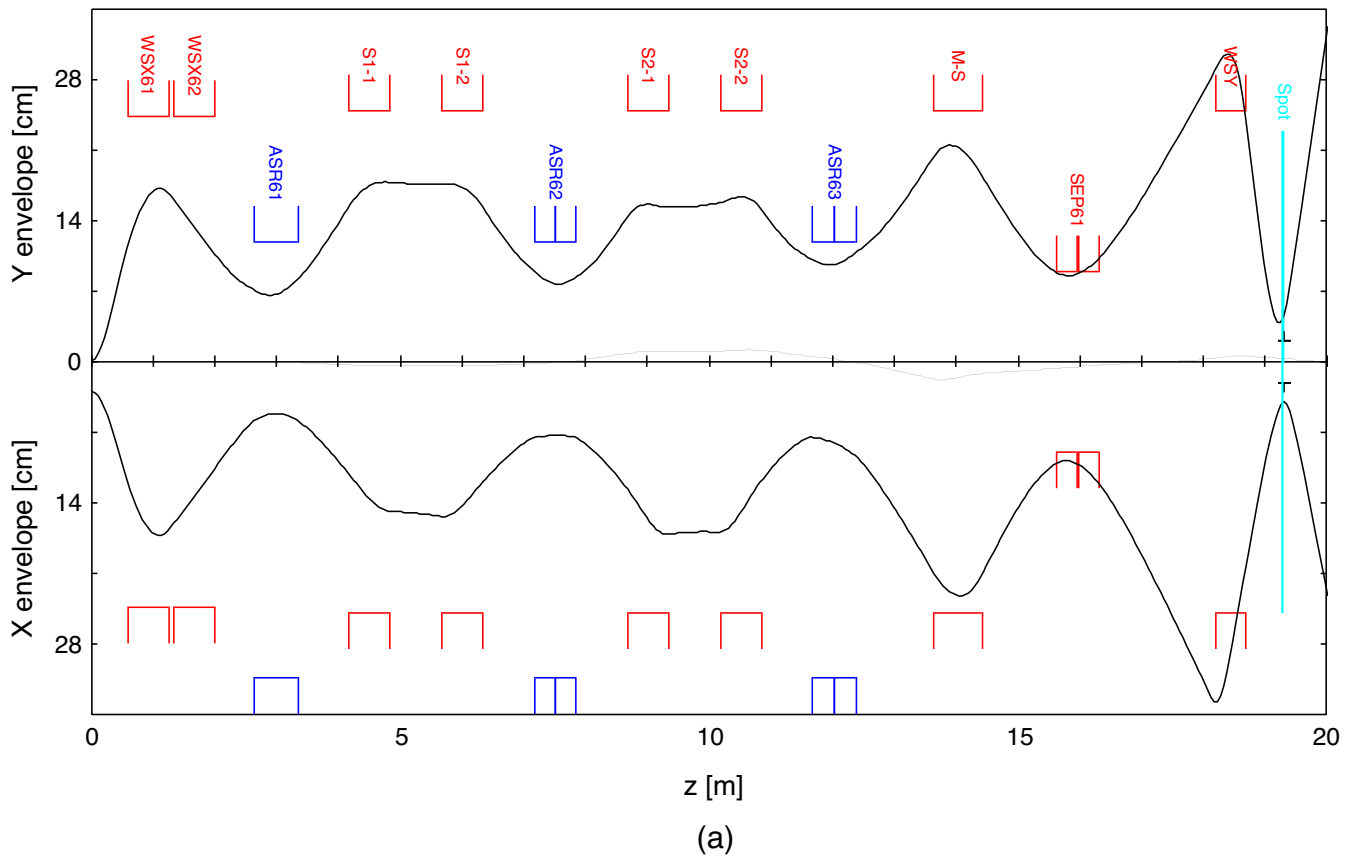| 15-keV muons		Fractions on area [mm^2]			
	Beam spot	5×5	10×10	20×20	25×25
Triplet	48 176	27.6%	65.2%	92.4%	95.9%
WSY, model-3	47 451	27.0%	65.1%	92.3%	96.0%

FIG. 23.   (a) Second-order optical calculation for the Super-μE4 in TRANSPORT. Initial parameters used in TRANSPORT are (half-width): $x = 30$ mm, $x' = 200$ mrad, $y = 2.5$ mm, $y' = 200$ mrad, $dp/p = 4.5\%$. (b) Beam envelopes ($2 \times$ rms) in multiparticle simulation after optimizing the magnetic fields using a homogeneous beam distribution at the source. Initial beam parameters as in (a).
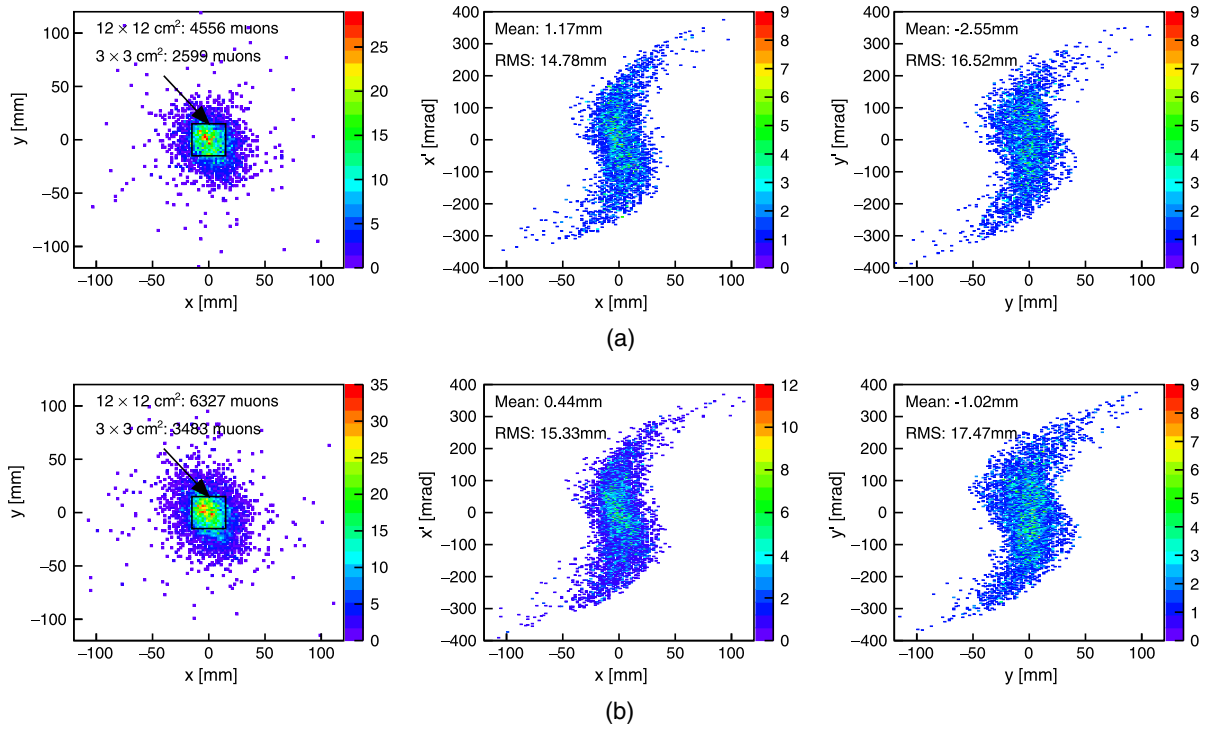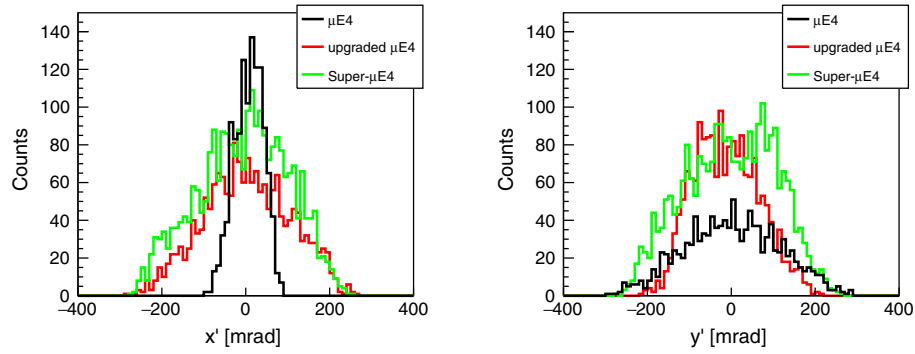
FIG. 24.   The beam spots for the Super-μE4 beamline: (a) with OTE; (b) with NTE.

FIG. 25.   Comparison of divergences for different beamline settings with the OTE.

muon rate on moderator by 42%, Super-μE4 yields an additional increase of about 55% for both, OTE and NTE. Overall, with the help of NTE, the Super-μE4 beamline can increase the muon beam rate on the moderator by a factor of 2.9 compared to the original intensity of the LEM facility with OTE.

TABLE II.   Comparison of the simulated beam intensity of the μE4 beam at the moderator position for different target and beamline settings.

	μE4		Upgraded μE4 (model-3 WSY)		Super-μE4	
	Beam spot	Moderator	Beam spot	Moderator	Beam spot	Moderator
OTE	2949	1186	2593	1685	4556	2599
NTE	4037	1577	4021	2235	6327	3483

V. CONCLUSIONS

Different methods of upgrading the surface muon beamline μE4 have been investigated. The feasibility of replacing the last quadrupole triplet with a specially designed solenoid has been demonstrated where the influence of its minimized stray field on the LEM beam transport is negligible. In the simulation, this new solenoid (model-3 WSY) results in an increase of 42% of surface muon beam rate on the moderator, which is 7% less compared to the G4beamline solenoid for OTE due to the shielding changing the stray field. With the NTE, routinely used in operation since 2021, the current μE4 beamline gains 33% in surface beam rate in the simulation, in good agreement with the measured increase in muon rate. The overall beam rate on moderator for model-3 WSY and NTE can be expected to increase by a factor of $\sim$1.9 compared to the current μE4 and OTE. In general, the lower transmission efficiency of surface muon beamlines composed of quadrupole magnets can be overcome by the employment of solenoids. Also benefiting from larger aperture solenoids, the Super-μE4 can deliver about 55% more muons to the end of the beamline, with a corresponding increase of muon rate on moderator. Compared to the current μE4 beamline, the rate on moderator increases by a factor of 2.2, for either OTE or NTE. The gain in muon rate on moderator of Super-μE4/NTE compared to the original μE4/OTE is $\sim$2.9.

Our study demonstrates the feasibility of upgrading existing surface muon beams by replacing conventional quadrupole doublets or triplets by normal-conducting, large aperture solenoids to significantly improve the beam intensity at the end of the beamline. The last focusing solenoid can be critical for experiments due to the usually large stray magnetic fields. These stray fields can be minimized by a special solenoid design with iron housing and built-in compensation coils, while maintaining its large focusing power.

APPENDIX: COMPARISON OF SIMULATED AND MEASURED MUON RATES

One can use the simulated numbers of Table II to check the reliability of the used QGSP_BIC model for pion

TABLE III. Comparison of muon rates, normalized to a proton beam current of 1 mA for the current μE4, OTE. The experimental data are from Ref. [3]. The simulation uses the BIC model for pion production.

	Muon rate on beam spot [1/mAs]	Muon rate on moderator [1/mAs]
Experiment	210×10^6	86×10^6
Simulation	184×10^6	74×10^6

production and the G4Beamline transport for predicting the observed muon rates in the entire beam spot and on the moderator. The simulation used 10^{11} protons on target. In the experiment [3], muon rates are given normalized to proton beam current of 1 mA, i.e., 1/mAs. A charge of 1 mAs corresponds to 6.25×10^{15} protons. Thus, scaling the numbers of Table II by 6.25×10^4 yields the simulated muon rates in Table III. Using the QGSP_BIC model, the muon rates are underestimated by 13%–14% compared to the experimental results. This originates from an underestimation of the BIC (Binary Cascade Model) pion production cross section relative to the measured production cross sections [26], where the enhanced measured pion production cross sections resulted in an even better agreement between simulated and measured beam rates. These results demonstrate the reliability of our beam transport simulation.

[1] F. Foroughi, E. Morenzoni, T. Prokscha, M. Daum, K. Deiters, D. George, D. Herlach, C. Petitjean, D. Renker, and V. Vrankovic, Upgrading the PSI muon facility, Hyperfine Interact. **138**, 483 (2001).

[2] T. Prokscha, E. Morenzoni, K. Deiters, F. Foroughi, D. George, R. Kobler, and V. Vrankovic, A new high-intensity, low-momentum muon beam for the generation of low-energy muons at PSI, Hyperfine Interact. **159**, 385 (2005).

[3] T. Prokscha, E. Morenzoni, K. Deiters, F. Foroughi, D. George, R. Kobler, A. Suter, and V. Vrankovic, The new μE4 beam at PSI: A hybrid-type large acceptance channel for the generation of a high intensity surface-muon beam, Nucl. Instrum. Methods Phys. Res., Sect. A **595**, 317 (2008).

[4] E. Morenzoni, H. Glückler, T. Prokscha, H. P. Weber, E. M. Forgan, T. J. Jackson, H. Luetkens, C. Niedermayer, M. Pleines, M. Birke, A. Hofer, J. Litterst, T. Riseman, and G. Schatz, Low-energy μ at PSI: present and future, Physica (Amsterdam) **289B**, 653 (2000).

[5] E. Morenzoni, R. Khasanov, H. Luetkens, T. Prokscha, A. Suter, N. Garifianov, H. Glückler, M. Birke, E. Forgan, H. Keller, J. Litterst, C. Niedermayer, and G. Nieuwenhuys, Low energy muons as probes of thin films and near surface regions, Physica (Amsterdam) **326B**, 196 (2003).

[6] T. Prokscha, E. Morenzoni, A. Suter, R. Khasanov, H. Luetkens, D. Eshchenko, N. Garifianov, E. M. Forgan, H.

Keller, J. Litterst, C. Niedermayer, and G. Nieuwenhuys, Thin Film, Near-Surface and Multi-Layer Investigations by Low-Energy μ^+SR, Hyperfine Interact. **159**, 227 (2005).

[7] E. Morenzoni, T. Prokscha, A. Suter, H. Luetkens, and R. Khasanov, Nano-scale thin film investigations with slow polarized muons, J. Phys. Condens. Matter **16**, S4583 (2004).

[8] T. Prokscha, E. Morenzoni, C. David, A. Hofer, H. Glückler, and L. Scandella, Moderator gratings for the generation of epithermal positive muons, Appl. Surf. Sci. **172**, 235 (2001).

[9] R. Xiao, E. Morenzoni, Z. Salman, B. J. Ye, and T. Prokscha, A segmented conical electric lens for optimization of the beam spot of the low-energy muon facility at PSI: A Geant4 simulation analysis, Nucl. Sci. Tech. **28**, 29 (2017).

[10] K. S. Khaw, A. Antognini, P. Crivelli, K. Kirch, E. Morenzoni, Z. Salman, A. Suter, and T. Prokscha, Geant4 simulation of the PSI LEM beam line: energy loss and muonium formation in thin foils and the impact of unmoderated muons on the μSR spectrometer, J. Instrum. **10**, P10025 (2015).

[11] A. D. Hillier, D. J. Adams, P. J. Baker, A. Bekasovs, F. C. Coomer, S. P. Cottrell, S. D. Higgins, S. J. S. Jago, K. G. Jones, J. S. Lord, A. Markvardsen, P. G. Parker, J. N. T. Peck, F. L. Pratt, M. T. F. Telling, and R. E. Williamson, Developments at the ISIS muon source and the concomitant benefit to the user community, J. Phys. Conf. Ser. **551**, 012067 (2014).

[12] A. D. Hillier, J. S. Lord, K. Ishida, and C. Rogers, Muons at ISIS, Phil. Trans. R. Soc. A **377**, 20180064 (2019).

[13] R. Abramishvili *et al.* (COMET Collaboration), COMET Phase-I technical design report, Prog. Theor. Exp. Phys. **2020**, 033C01 (2020).

[14] S. Cook, R. D'Arcy, A. Edmonds, M. Fukuda, K. Hatanaka, Y. Hino, Y. Kuno, M. Lancaster, Y. Mori, T. Ogitsu, H. Sakamoto, A. Sato, N. H. Tran, N. M. Truong, M. Wing, A. Yamamoto, and M. Yoshida, Delivering the world's most intense muon beam, Phys. Rev. Accel. Beams **20**, 030101 (2017).

[15] D. Tomono *et al.*, Muon beamline commissioning and feasibility study for μSR at a new DC muon beamline, MuSIC-RCNP, Osaka University, J. Phys. Soc. Jpn. Conf. Proc. **21**, 011057 (2018).

[16] P. Strasser, Y. Ikedo, S. Makimura, J. Nakamura, K. Nishiyama, K. Shimomura, H. Fujimori, T. Adachi, A. Koda, N. Kawamura, Y. Kobayashi, W. Higemoto, T. U. Ito, T. Nagatomo, E. Torikai, R. Kadono, and Y. Miyake, Design and construction of the ultra-slow muon beamline at J-PARC/MUSE, J. Phys. Conf. Ser. **551**, 012065 (2014).

[17] J. Nakamura, T. Nagatomo, Y. Oishi, Y. Ikedo, P. Strasser, N. Saito, K. Miyazaki, K. Yokoyama, K. Okamura, Y. Miyake, S. Makimura, K. Nishiyama, K. Shimomura, N. Kawamura, A. Koda, W. Higemoto, S. Wada, M. Iwasaki, and E. Torikai, Ultra slow muon microscope at MUSE/J-PARC, J. Phys. Conf. Ser. **502**, 012042 (2014).

[18] Y. Ikedo *et al.*, The status of the superomega muon beamline, in *Proceedings of the 12th International Workshop on Neutrino Factories, Superbeams, and Betabeams: NuFact10*, edited by B. S. Acharya, M. Goodman, and N. K. Mondal, AIP Conf. Proc. No. 1382 (AIP, New York, 2011), pp. 220–222, 10.1063/1.3644317.

[19] K. Nakahara, Y. Miyake, K. Shimomura, P. Strasser, K. Nishiyama, N. Kawamura, H. Fujimori, S. Makimura, A. Koda, K. Nagamine, T. Ogitsu, A. Yamamoto, T. Adachi, K. Sasaki, K. Tanaka, N. Kimura, Y. Makida, Y. Ajima, K. Ishida, and Y. Matsuda, The super omega muon beamline at J-PARC, Nucl. Instrum. Methods Phys. Res., Sect. A **600**, 132 (2009).

[20] Y. Miyake *et al.*, J-PARC muon facility, MUSE, J. Phys. Soc. Jpn. Conf. Proc. **21**, 011054 (2018).

[21] N. Kawamura, M. Aoki, J. Doornbos, T. Mibe, Y. Miyake, F. Morimoto, Y. Nakatsugawa, M. Otani, N. Saito, Y. Seiya, K. Shimomura, A. Toyoda, and T. Yamazaki, New concept for a large-acceptance general-purpose muon beamline, Prog. Theor. Exp. Phys. **2018**, 113G01 (2018).

[22] A. Papa, Towards an high intensity muon beam (HiMB) at PSI, https://indico.cern.ch/event/577856/contributions/3420391/attachments/1879682/3097488/Papa_HiMB_EPS2019.pdf (2019).

[23] K. S. Kirch, Welcome report at Open User Meeting BV51, https://indico.psi.ch/event/8337/contributions/22169/attachments/16011/22593/KK-BVR2020.pdf (2020).

[24] M. Aiba *et al.*, Science case for the new high-intensity muon beams HIMB at PSI, arXiv:2111.05788.

[25] J. Tang *et al.*, EMuS muon facility and its application in the study of magnetism, Quantum Beam Sci. **2**, 23 (2018).

[26] F. Berg, L. Desorgher, A. Fuchs, W. Hajdas, Z. Hodge, P. R. Kettle, A. Knecht, R. Lüscher, A. Papa, G. Rutar, and M. Wohlmuther, Target studies for surface muon production, Phys. Rev. Accel. Beams **19**, 024701 (2016).

[27] D. M. Kaplan and T. J. Roberts, G4beamline simulation program for matter-dominated beamlines, in *Proceedings of the 22nd Particle Accelerator Conference, PAC-2007, Albuquerque, NM* (IEEE, New York, 2007), p. 3468, 10.1109/PAC.2007.4440461.

[28] M. Eshraqi, G. Franchetti, and A. M. Lombardi, Emittance control in rf cavities and solenoids, Phys. Rev. Accel. Beams **12**, 024201 (2009).

[29] PSI Graphic Transport Framework, by U. Rohrer based on a CERN-SLAC-FERMILAB version by K. L. Brown *et al.*

[30] Opera: A finite element analysis software suite developed by Dassault Systèmes, https://www.3ds.com/products-services/simulia/products/opera/.

[31] V. Kumar, Understanding the focusing of charged particle beams in a solenoid magnetic field, Am. J. Phys. **77**, 737 (2009).

[32] R. E. Laxdal, Review of magnetic shielding designs of low-beta cryomodules, in *Proceedings of the 16th International Conference on RF Superconductivity (SRF 2013), Paris, France* (JACoW, Geneva, Switzerland, 2013), https://accelconf.web.cern.ch/SRF2013/papers/weiod01.pdf.

[33] T. Takeuchi, Magnetic field of a double-layer solenoid, Phys. Teach. **35**, 306 (1997).

[34] K. Sedlak, R. Scheuermann, T. Shiroka, A. Stoykov, A. Raselli, and A. Amato, MusrSim and MusrSimAna–Simulation tools for μSR instruments, Phys. Procedia **30**, 61 (2012).